

N. I. Elkalashy, M. Lehtonen, H. A. Darwish, A.-M. I. Talaab and M. A. Izzularab, DWT-Based Extraction of Residual Currents Throughout Unearthed MV Networks for Detecting High-Impedance Faults Due to Leaning Trees, European Transactions on Electrical Power, ETEP, vol. 17, no. 6, pp. 597-614, November/December 2007.

© 2007 John Wiley & Sons

Reproduced with permission.

DWT-based extraction of residual currents throughout unearthed MV networks for detecting high-impedance faults due to leaning trees

Nagy I. Elkalashy^{1,*†}, Matti Lehtonen¹, Hatem A. Darwish², Abdel-Maksoud I. Taalab² and Mohamed A. Izzularab²

¹*Power Systems & High Voltage Engineering, Helsinki University of Technology (TKK), Otakaari 5 I, Otaniemi, Espoo, PO Box 3000, FI-02015 HUT, Finland*

²*Electrical Engineering Department, Faculty of Engineering, Minoufiya University, Shebin El-Kom 32511, Egypt*

SUMMARY

Modelling of a high-impedance arcing fault due to a leaning tree in medium voltage (MV) networks was experimentally verified and the network transients due to this fault were also investigated. Even though the tree had a very high resistance value, the initial transients were periodically caused by the arc reignitions after each zero-crossing. In this paper, these features are extracted from residual currents using discrete wavelet transform (DWT) to localise this fault event. The DWT performance at different measuring nodes throughout an unearthed 20 kV network can be gathered at the base station using wireless sensors concept. So, the DWT is evaluated for a wide area of the network and the fault detection is confirmed by numerous DWT extractors. Due to the periodicity of arc reignitions, the initial transients are localised not only at fault starting instant but also during the fault period that will enhance the detection security. The term of locating the faulty section is determined based on ratios of the residual current amplitudes. The fault cases are simulated by ATP/EMTP and the arc model is implemented using the universal arc representation. Copyright © 2007 John Wiley & Sons, Ltd.

KEY WORDS: arc modelling; discrete wavelet transform; high-impedance arcing fault; wireless sensors

1. INTRODUCTION

In electrical distribution networks, reliable detections of high-impedance faults are significant problems [1–3]. The detection difficulty is due to small impacts of these faults on the electrical quantities. When they are associated with arcs, it becomes hazardous for both human beings and electrical equipments as well.

All researching efforts directed to detect such faults show the way to understand their features and the practical considerations for their detection [4–10]. The features are extracted using several digital filters such as Fast Fourier Transform (FFT), Kalman filter, Fractal and Wavelet Transform [4–7].

*Correspondence to: Nagy I. Elkalashy, Power Systems & High Voltage Engineering, Helsinki University of Technology (TKK), Otakaari 5 I, Otaniemi, Espoo, PO Box 3000, FI-02015 HUT, Finland.

†E-mail: n_ekalashy@yahoo.com

Therefore, several detection algorithms have been motivated depending on harmonic contents such as second order, third order, composite odd harmonics, even harmonics, nonharmonics, high frequency spectra and harmonic phase angle considerations [7–9]. Multiple algorithms can enhance the fault detection [10]. However, such techniques are not applied for identifying the faults due to a leaning tree.

The faults due to a leaning tree are also categorised as a high-impedance fault due to the high resistance of the tree (several hundred ohms) and they are also associated with arcs [1]. Since the electrical network in the Nordic countries is exposed to the leaning trees as a result of large forest areas, it is worthwhile to study the detection of this fault. The fault due to a leaning tree has been previously modelled in Reference [1] and its corresponding initial transients of the network have been discussed in Reference [2].

The transients produced in electrical networks due to faults often depend on the neutral point treatments. They can be completely isolated from ground, earthed through impedance or solidly earthed at their neutral. In Nordic Countries, the neutral is commonly unearthed and the compensated medium voltage (MV) networks have increasingly being used [11]. The system used in this study is a 20 kV unearthed network.

The wireless sensor concept is a modern insight used for various objects with saving time and expenses. The wireless sensor networks include compact microsensors and wireless communication capability. They are distributed in the network and electrical quantities are then frequently transmitted from different measuring points and investigated for several purposes such as load monitoring, fault detection and location, etc. [12–15].

In this paper, the impact of arc reignitions periodicity on the residual waveforms are used to detect the high-impedance fault due to a leaning tree. The initial transients in vicinity of the current zero-crossing lead to fingerprints enhancing the fault detection. These initial transients are localised based on discrete wavelet transform (DWT) to detect the fault. The wireless sensor concept is used for enhancing the fault detection and location processes. The ratio of the residual fundamental current of each section with respect to the parent section in the feeder is estimated for locating the faulty section. A practical 20 kV unearthed network is simulated in ATP/EMTP and using ATPDraw as a graphical interface. The fault model is incorporated at different locations in the network and the associated arc is implemented using the universal arc representation.

2. SIMULATED SYSTEM

The simulation of the electrical networks associated with high-impedance arcing faults is significant to evaluate the possibility of their discrimination. The system model can be divided into two main parts: the MV network model and representation of the high-impedance arcing fault described in the following subsection. Furthermore, the wireless sensors and their locations in the simulated network are discussed.

2.1. 20 kV MV network

Figure 1 illustrates the single line diagram of an unearthed 20 kV, 5 feeders distribution network simulated using ATP/EMTP, in which the processing is created by ATPDraw [16]. The feeder lines are represented using frequency dependent JMarti model type with considering the feeder configuration given in the Appendix.

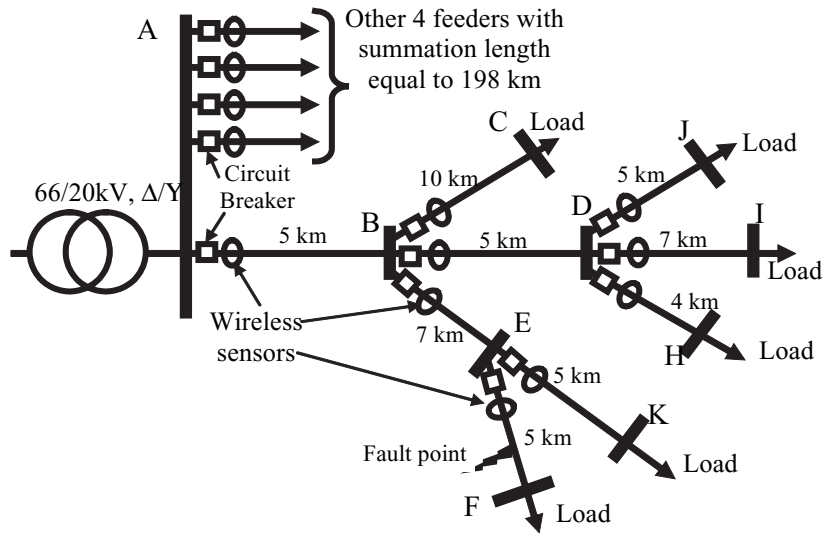


Figure 1. Simulated system for a substation energised 251 km distribution network (5 feeders).

The neutral of the main transformer is isolated to manage unearthed system. Although the ungrounded network is not intentionally connected to the earth, it is grounded by the natural phase to ground capacitances. Therefore, the phase fault current is very low allowing to a high continuity of service [11]. The main disadvantage of this network is that it is subjected to transient overvoltages. The current distributions in the unearthed networks during ground faults are addressed in References [11–12].

2.2. Fault modelling

An experiment was performed to measure the characteristics of a high-impedance arcing fault due to a leaning tree occurring in a 20 kV distribution network [1]. The fault is modelled using two series parts: a dynamic arc model and a high resistance. For the considered case study, the resistance is 140 k Ω [1]. Regarding the arc modelling, the most popular modelling rules depend on thermal equilibrium that has been adapted as [17]:

$$\frac{dg}{dt} = \frac{1}{\tau}(G - g) \quad (1)$$

$$G = \frac{|i|}{V_{\text{arc}}} \quad (2)$$

where g is the time-varying arc conductance, G is the stationary arc conductance, $|i|$ is the absolute value of the arc current, V_{arc} is a constant arc voltage parameter, and τ is the arc time constant. For representing the arc associated with this fault type, τ is changed to fit the new application as [1]:

$$\tau = Ae^{Bg} \quad (3)$$

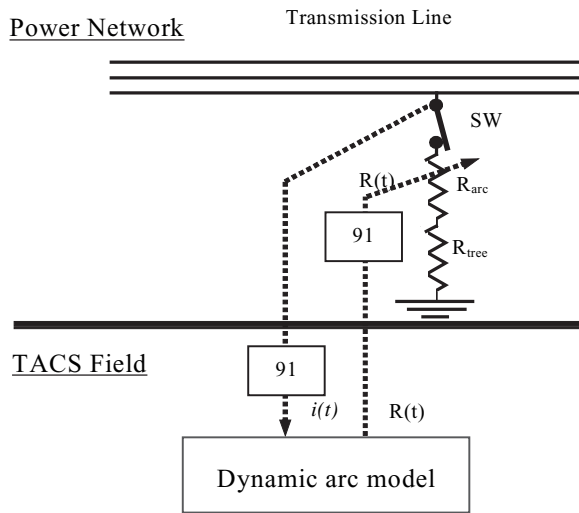


Figure 2. EMTP network of the high-impedance arcing fault.

where A and B are constants. In Reference [1], the parameters V_{arc} , A and B have been found to be 2520 V, $5.6E-7$ and 395917, respectively. Considering the conductance at each zero-crossing, the medium dielectric until instant of the reignition is represented by a variable resistance. It is represented using a ramp function of $0.5 \text{ M}\Omega/\text{millisecond}$ for a period of 1 millisecond after the zero-crossing and then $4 \text{ M}\Omega/\text{millisecond}$ until the reignition instants.

Considering the bilateral interaction between the EMTP power network and the transient analysis control system (TACS) field, the arcing Equations (1)–(3) are implemented using the universal arc representation [18]. With the help of Figure 2, the current is transposed into TACS field using sensors type 91. It is used as input to the arc model that is solved in the TACS exploiting integrator device type 58 with the aid of FORTRAN expressions. In the next step, the computed arc resistance is sent back into the network using TACS controlled resistance type 91 and so on. Accordingly, the arcing fault interaction and the corresponding transients are performed. Control signals are generated to distinguish between arcing and dielectric periods and therefore to fulfil the reignition instant after each zero-crossing. The aforementioned MV network and the fault modelling are combined in one arrangement as shown in ATPDraw circuit illustrated in the Appendix.

2.3. Wireless sensors network

Towards increasing the range of data gathering from the electrical network nodes to their main substation, the wireless sensor networks are recently constructed. The availability of sensing devices, embedded processors, communication kits and power equipment enables the design of wireless sensor as depicted from the illustrated four major blocks in Figure 3 [15]. The supply is used to power the node. The communication block consists of a wireless communication channel which can be short radio, laser, or infrared. The processing unit is composed of memory to store data and applications programs, a microcontroller (MCU) and an analog-to-digital converter (ADC) to receive signal from the sensing device. The sensing block links the sensor node to the physical conditions. In our

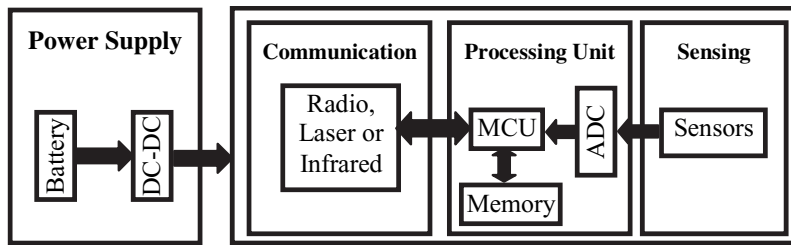


Figure 3. Architecture of the sensor node system [15].

application, the sensing device is used to measure the feeder line currents as deeply discussed in References [12–14].

New network protocols are necessary including link, network, transport and application layers to solve the problems like routing, addressing, clustering, synchronisation and they have to be energy-efficient [15]. This paper is not going into deeper exploration on such issues. The point of view is that the wireless concept is used for gathering the currents at different nodes in the network as depicted in Figure 1. The currents are investigated to detect the fault due to leaning trees.

3. FAULT TEST CASES

The best waveforms which can be analysed for detecting high-impedance ground faults occurring in unearthed distribution networks are the residual voltage and current waveforms. They are computed as:

$$u_r = u_a + u_b + u_c \quad (4)$$

$$i_r = i_a + i_b + i_c \quad (5)$$

where u_r , and i_r are the residual voltages and currents, respectively. u_a , u_b and u_c are the phase voltages. i_a , i_b and i_c are the phase currents. In order to investigate these residual waveforms during the highlighted fault, the residual currents using Equation (5) is implemented in the TACS field at different locations of the wireless sensors as depicted in the ATPDraw circuit.

Referring to the simulated system shown in Figure 1, the fault occurred at the end of section EF. The phase currents are collected at the substation A using the distributed wireless sensors and the residual current waveform of each section is shown in Figure 4. From the enlarged view, it is obvious that the higher residual current amplitude is the measured one in the faulty section and it is slightly reduced for each upstream section BE and AB. The initial transients of the other sections that are healthy are also obvious at each zero-crossing. This is because there are couplings between the network phases and the earth along with the feeders' lengths.

Figure 5 illustrates the residual currents for another fault case occurred at the end of section BD. In the same manner, the residual current of faulty section BD and consequently of the section AB are higher than the other healthy sections. Also, the initial transients associated with the arc reignitions have appeared in all residual current waveforms.

Although these perceptible discriminations in the performance of the residual current magnitudes during this fault can indicate for the faulty section, it is not suitable to depend on such magnitudes directly. It is because they are very small (less than 100 mA). However, the impact of arc reignitions on

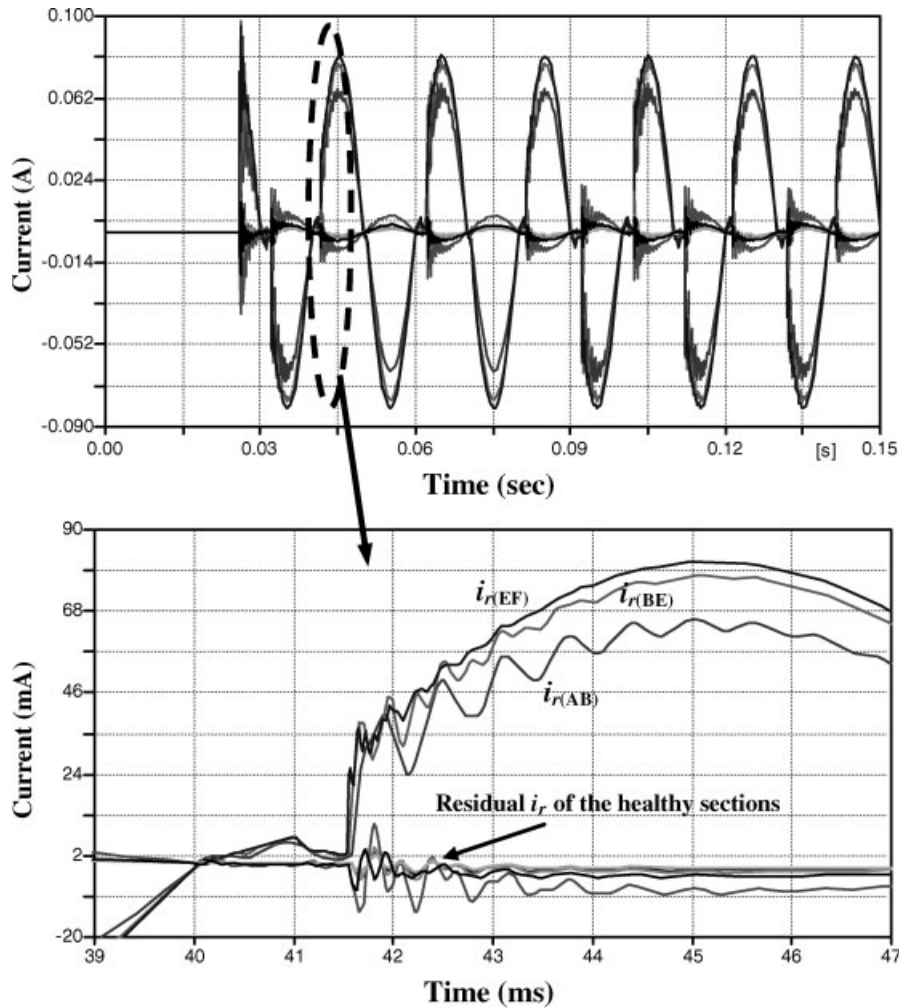


Figure 4. Enlarged view of residual current waveforms (i_r) when the fault occurred in section EF.

the residual waveforms is obvious and can be used for detecting the fault. The most suitable signal processing technique for localising these initial transients is DWT.

4. DWT-BASED FAULT DETECTION

Wavelets are families of functions generated from one single function, called the mother wavelet, by means of scaling and translating operations. The scaling operation is used to dilate and compress the mother wavelet to obtain the respective high and low frequency information of the function to be analysed. Then the translation is used to obtain the time information. In this way a family of scaled and translated wavelets is created and it serves as the base for representing the function to be analysed [19].

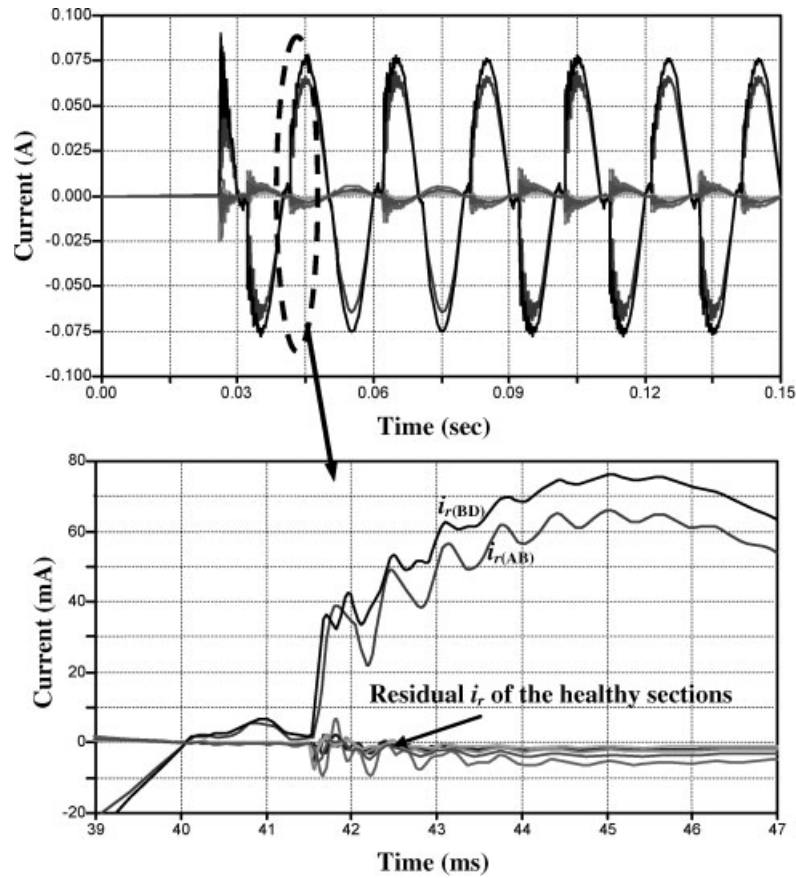


Figure 5. Enlarged view of residual current waveforms (i_r) when the fault occurred in section BD.

The DWT is in form:

$$\text{DWT}_{\psi} f(m, k) = \frac{1}{\sqrt{a_0^m}} \sum_n x(n) \psi\left(\frac{k - nb_0 a_0^m}{a_0^m}\right) \quad (6)$$

where $\psi(\cdot)$ is the mother wavelet that is discretely dilated and translated by a_0^m and $nb_0 a_0^m$, respectively, where a_0 and b_0 are fixed values with $a_0 > 1$ and $b_0 > 0$. m and n are integers. In the case of the dyadic transform, which can be viewed as a special kind of DWT spectral analyser, $a_0 = 2$ and $b_0 = 1$. DWT can be implemented using a multi-stage filter with down sampling of the output of the low-pass filter. The practical realisation of the DWT is addressed in Reference [20], in which its experimental implementation was accomplished using DSP board (DSP1003) with reducing its lengthy execution time.

Several wavelet families have been tested to extract the fault features using the Wavelet toolbox incorporated into the MATLAB program [21]. Daubechies wavelet 14 (db14) is appropriate to localise this fault. Details d3, d4 and d5 including the frequency bands 12.5–6.25, 6.25–3.125 and 3.125–1.5625 kHz are investigated where the sampling frequency is 100 kHz. It is evident from these

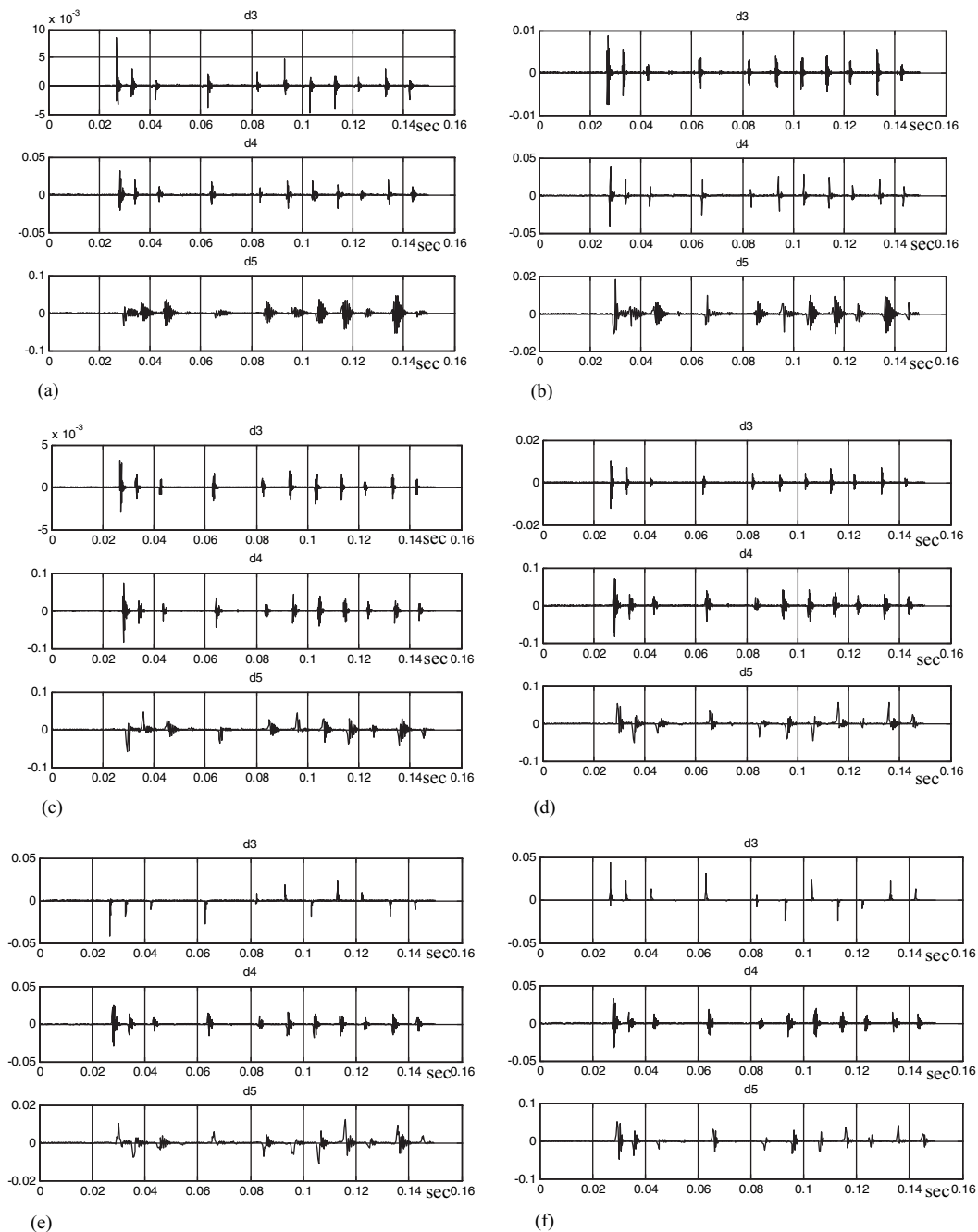


Figure 6. Details of residual waveforms shown in Figure 4. (a) Details of the residual current in section AB ($i_{r(AB)}$), (b) Details of the residual current in section Bc ($i_{r(BC)}$), (c) Details of the residual current in section BD ($i_{r(BD)}$), (d) Details of the residual current in section BE ($i_{r(BE)}$), (e) Details of the residual current in section EK ($i_{r(EK)}$), (f) Details of the residual current in section EF ($i_{r(EF)}$).

frequency bands that the sampling frequency can be reduced. However, details d1 and d2 are not used to avoid the field noise effect [20]. For the fault case occurred at the end of section EF and depicted in Figure 4, features of the residual currents at different locations are analysed as shown in Figure 6. It is obvious that the initial transients due to arc reignitions are frequently localised at each zero-crossing.

To find flags used as fault detectors, the average summation of the absolute values of each detail over a window of the power frequency is computed in a discrete form as:

$$S_{di}(k) = \frac{1}{N} \sum_{h=k-N+1}^k |di(h)| \quad (7)$$

where $S_{di}(k)$ means the detector in discrete samples according to the detail levels di such as S_{d3} , S_{d4} and S_{d5} corresponding to details d3, d4 and d5. h is used for carrying out a sliding window covering 20 milliseconds with N a number of samples.

The performance of the detectors S_{di} for different measuring locations is shown Figure 7. It can be said that the fault is detected based on DWT. Moreover, the considered detectors are high not only at the starting instant of the fault events but also during the fault period. However, a threshold value equal to 0.01 is considered to discriminate between this fault case and the measurement noises. This threshold value $S_{di} > 0.01$ is evident with the aid of the experimental waveforms of this fault current and voltage illustrated in Reference [1]. In this Reference, the experimental waveforms processed using DWT with the same mother wavelet Daubechies 14 (db14) for comparison purposes. It is found that the fault features are extracted using the experimental data considering details d3 and d4 and there is a good agreement with the simulation results. By applying the discriminator S_{di} Equation (7) on the DWT details d3 and d4 of the experimental fault currents in Reference [1], it is found that a threshold value is equal to 0.01 to discriminate between the fault features and noises. (Figure 8)

5. FAULTY SECTION DISCRIMINATION

It should be noted that the aforementioned detectors can only identify the high-impedance fault due to a leaning tree, however, they cannot discriminate the faulty section. In order to overcome this shortcoming, the ratio of the fundamental component of each section with respect to the parent section is computed. Therefore, the fundamental component is tracked using a recursive Discrete Fourier Transform (DFT) as:

$$I_{\text{real}} = I_{\text{real}} + \frac{2}{N} (i_r(k) - i_r(k - N)) \cos(k\theta) \quad (8)$$

$$I_{\text{imaj}} = I_{\text{imaj}} + \frac{2}{N} (i_r(k) - i_r(k - N)) \sin(k\theta) \quad (9)$$

$$I_r = \sqrt{I_{\text{real}}^2 + I_{\text{imaj}}^2} \quad (10)$$

where $\theta = 2\pi/N$, $i_r(k)$ is the discrete input samples of the residual current and I_{real} , I_{imaj} and I_r are the in-phase, quadrature-phase and the amplitude, respectively. The corresponding fundamental amplitudes of the residual current waveforms of different sections are shown in Figure 8. It illustrates that the residual current amplitudes of sections AB, BE and EF are the higher than the others. Accordingly, the ratio of the residual fundamental current component of each section with respect to

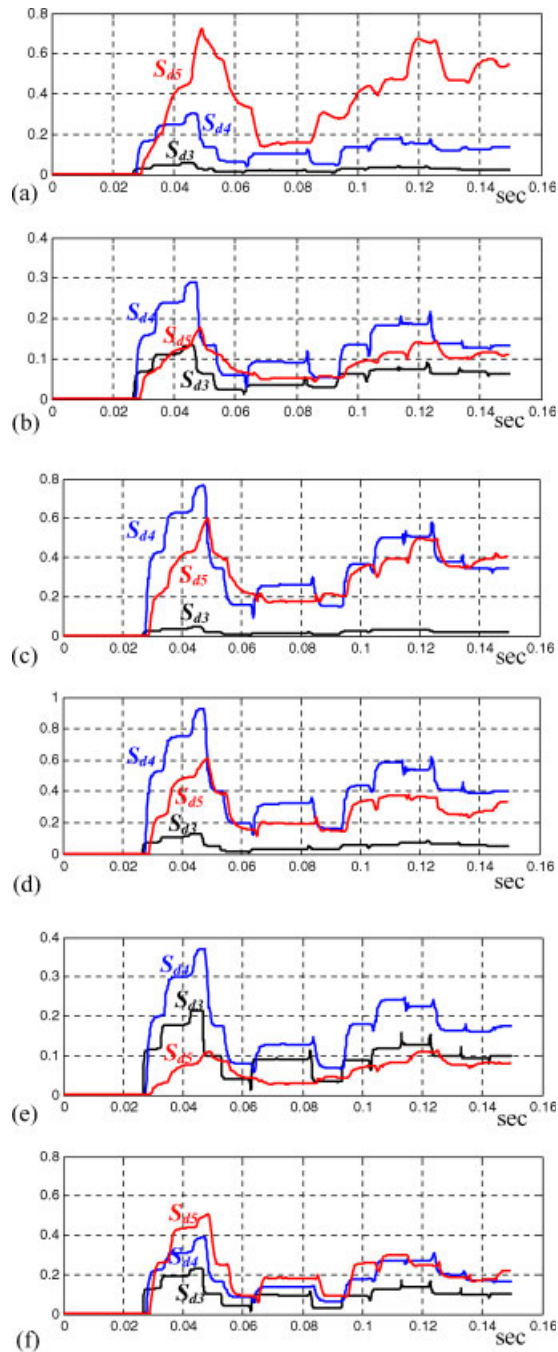


Figure 7. The detector S_{di} of the details shown in Figure 6. (a) S_{di} of the residual current details in section AB ($i_{r(AB)}$), (b) S_{di} of the residual current details in section BC ($i_{r(BC)}$), (c) S_{di} of the residual current details in section BD ($i_{r(BD)}$), (d) S_{di} of the residual current details in section BE ($i_{r(BE)}$), (e) S_{di} of the residual current details in section EK ($i_{r(EK)}$), (f) S_{di} of the residual current details in section EF ($i_{r(EF)}$).

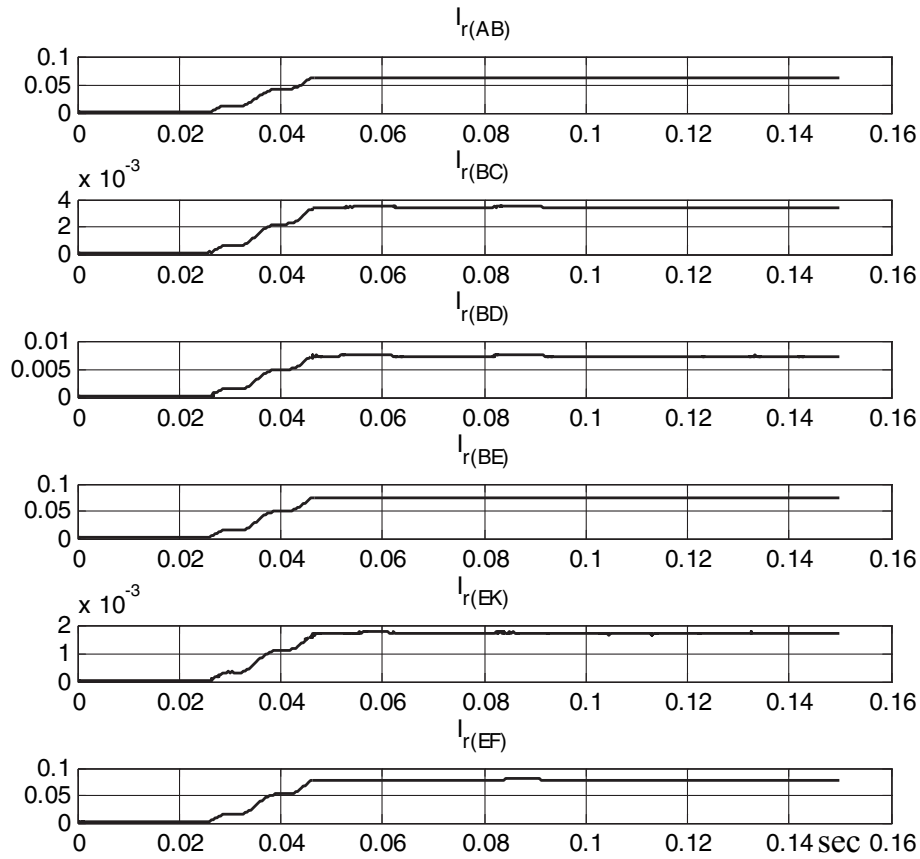


Figure 8. Fundamental components of the residual currents shown in Figure 5.

the residual current amplitude of the parent section AB is computed to estimate the fault path. For example, the ratio regarding section EK is:

$$R_{EK} = \frac{I_{r(EK)}}{I_{r(AB)}} \quad (11)$$

where $I_{r(EK)}$ and $I_{r(AB)}$ are the fundamental residual current components of sections EK and AB, respectively. Similarly, ratios regarding other sections are computed and the corresponding performances are shown in Figure 9. Due to the fault in section EF, the ratios R_{BE} and R_{EF} are the highest and they are approximately equal to one during the fault. Before the fault, the ratios are not stable because the value of residual current of section AB is approximately zero. However, they are only considered during the detectors S_{di} indicating for the fault existence.

Towards increasing the fault location security, the aforementioned ratio is computed for the change of residual current amplitudes. This change is the difference between the residual current magnitude

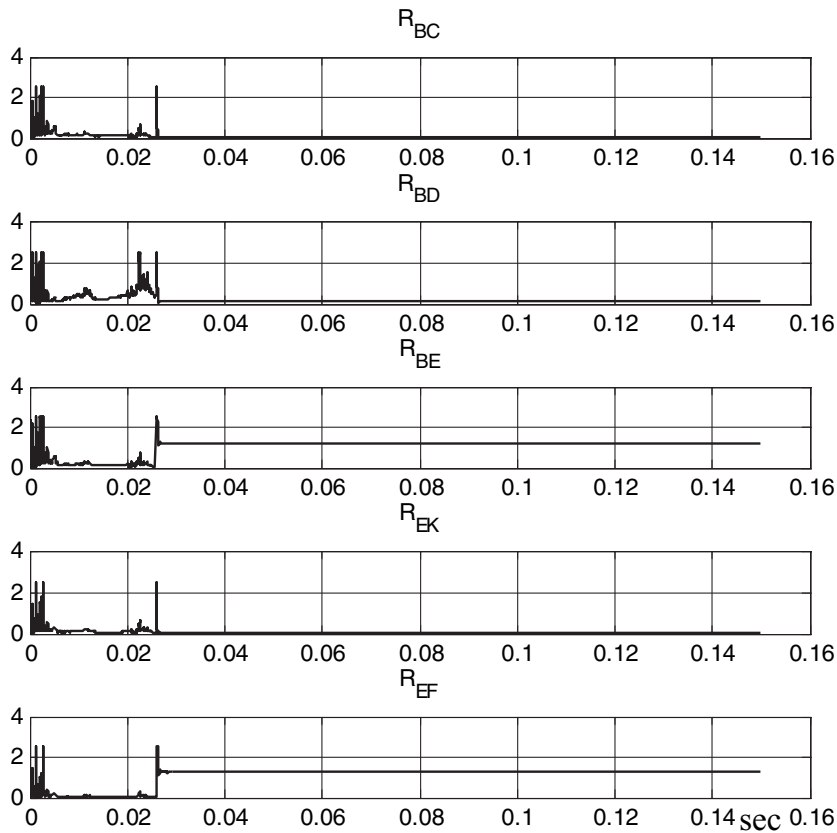


Figure 9. Discriminators R for the fault case shown in Figure 5.

during and pre-fault measurements. For example, the ratio of section EK is computed as:

$$R'_{EK} = \frac{\Delta I_{r(EK)}}{\Delta I_{r(AB)}} = \frac{I_{r(EK)\text{during}} - I_{r(EK)\text{pre}}}{I_{r(AB)\text{during}} - I_{r(AB)\text{pre}}} \quad (12)$$

For applying these discriminators, distinguishing between pre-fault and during the fault periods should be carried out and can be managed using the detectors shown in Figure 7. As soon as the fault features extracted by DWT are appeared, the R' discriminator is expected to locate the faulty section.

6. DISCUSSION

The scenario of this fault detection and its location can be generalised by Figure 10. At each measuring node, the phase currents (i_a , i_b , i_c) are measured and the residual current is computed. The residual current is then processed using DWT to compute the detector S_{di} . If S_{di} is greater than 0.01, then the fault exists.

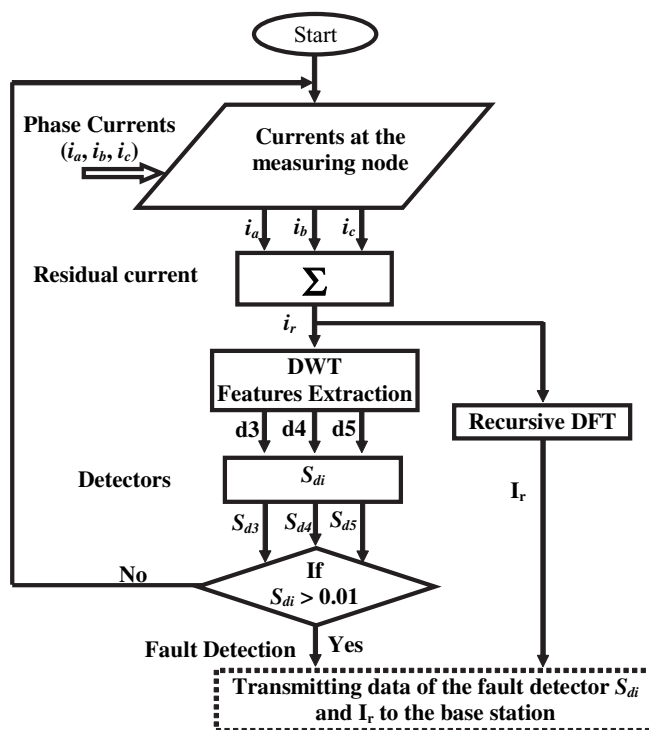


Figure 10. The proposed detection technique.

The fundamental current component I_r is computed using the recursive DFT. Once the fault is detected, the detectors S_{di} and I_r are transmitted to the base station using the wireless communication channels. The data transmission can be accomplished at a lower sampling rate. The detectors S_{di} are suitable to discriminate between periods of pre-fault and during the fault to apply the discriminator function R' . Designing appropriate logic functions or artificial intelligent techniques considering the detectors S_{di} and discriminators R' of each section as inputs are required for an adaptive faulty section locator.

Towards decreasing the sampling frequency at which the DWT is processed, it is evident from Figure 7 that the detail d4 is the most suitable coefficient when it is used for detecting the fault. So, the sampling frequency can be reduced to 50, 25 or 12.5 kHz; however, the used coefficient will be detail d3, d2 or d1, respectively.

Furthermore, the fault due to a leaning tree circumstances are controlled by the tree movement and wind speed. So, this fault with the obtained features can be diminished due to tree moving far away from the electrical conductor. When the tree is leaned again towards the conductor, these features will be more repeated. Therefore, the repetitions of detecting this fault type will also enhance the fault detection security.

7. CONCLUSIONS

A novel detection technique of a high-impedance arcing fault caused by leaning trees has been proposed based on extracting the residual current waveforms using DWT. Therefore, the current

sensors are only required disregarding voltage sensors. The fault model has been incorporated in different locations in 20 kV network using the ATP/EMTP program, where the network has been pre-processed by ATPDraw. The residual currents have been computed for each electrical section in the feeder, in which the phase currents have been measured using the allocated wireless sensors. The periodicity of the arc reignitions has given a significant performance for the DWT with this fault type and the results ascertain the fault detection. The faulty section has been estimated by the ratios of the residual current change in each electrical section with respect to the residual current change in the parent section. A sensitive and secure detection of the faults due to a leaning tree has been attained using DWT and wireless sensor concept.

8. LIST OF SYMBOLS AND ABBREVIATIONS

MV	medium voltage
DWT	discrete wavelet transform
MCU	microcontroller
ADC	analog-to-digital converter
g	time-varying arc conductance
G	stationary arc conductance
$ i $	absolute value of the arc current
V_{arc}	a constant arc voltage parameter
τ	arc time constant
A and B	constants
EMTP	electromagnetic transient program
ATP	alternative transient program
TACS	transient analysis control system
u_r	residual voltage
i_r	residual currents
u_a, u_b, u_c	phase voltages
i_r, i_a, i_b	phase currents
$\psi(\cdot)$	mother wavelet
a_o^m	dilation
$nb_o a_o^m$	translation,
a_o and b_o	fixed values with $a_o > 1$ and $b_o > 0$
m and n	integers
db14	Daubechies wavelet 14
$S_{\text{di}}(k)$	the detector in discrete samples
h	counter for carrying out a sliding window covering 20 milliseconds
N	a number of samples
I_{real}	in-phase value component
I_{imag}	quadrature-phase component
I_r	current amplitude
R	a ratio of the residual fundamental current component of each section with respect to the residual current amplitude of the parent section AB
$I_{r(\cdot)\text{pre}}$	pre-fault residual current
$I_{r(\cdot)\text{during}}$	during-fault residual current

APPENDIX

Figure 11 illustrates the considered ATPDraw network. It contains the MV network as described in Figure 1, the universal arc representation which is illustrated in Figure 4 and the residual currents (i_r) which are described by Equation (4). The feeders are represented using frequency-dependent JMarti model, the configuration of which is shown in Figure 12.

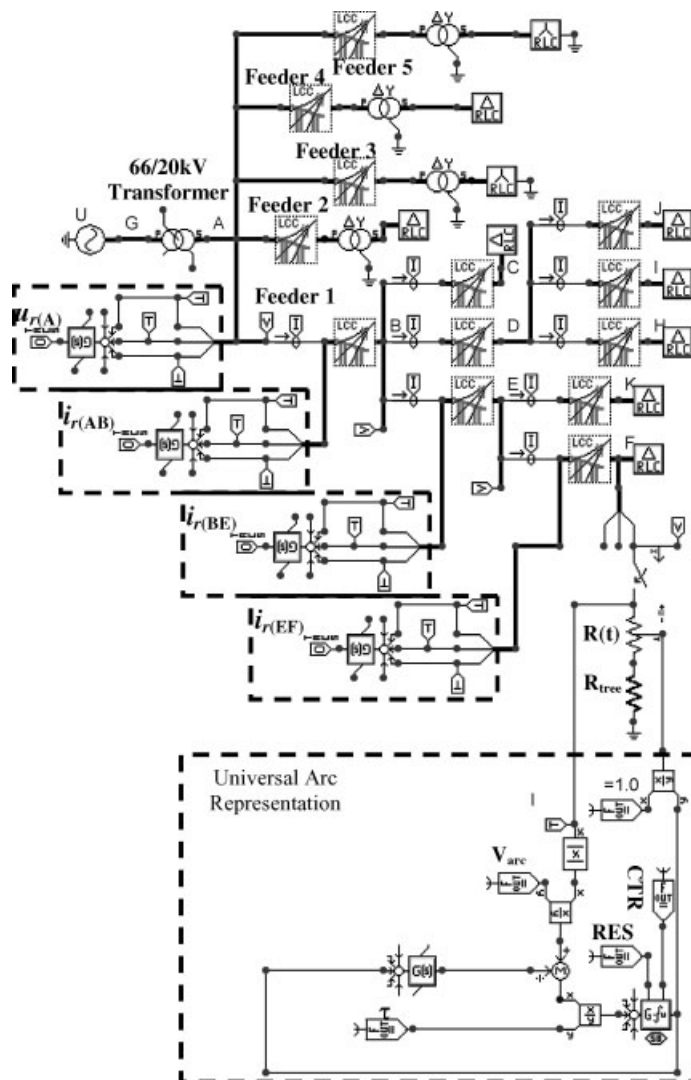


Figure 11. The ATPDraw network.

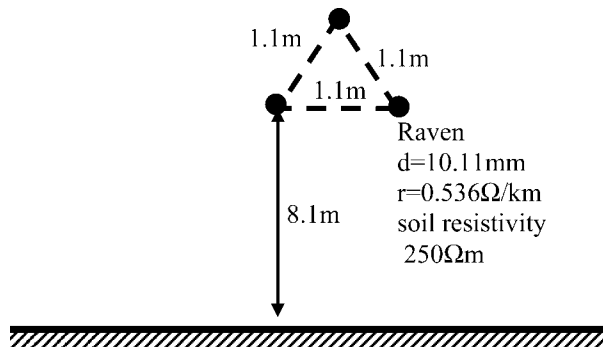


Figure 12. The feeder configuration.

ACKNOWLEDGEMENTS

The authors gratefully acknowledge the discussions with Mr. Asaad Elmoudi and Mr. G. Murtaza Hashmi.

REFERENCES

1. Elkalashy N, Lehtonen M, Darwish H, Izzularab M, Taalab A. Modeling and Experimental Verification of a High Impedance Arcing Fault in MV Networks. *IEEE/PES, Power Systems Conference and Exposition, PSCE2006*, 27 Oct–1 Nov 2006, Atlanta, Georgia, USA.
2. Elkalashy N, Lehtonen M, Darwish H, Taalab A, Izzularab M. Electromagnetic Transients due to a High Impedance Arcing Fault in MV Networks. *International Conference on Electromagnetic Disturbances, EMD 2006*, 27–29 Sep, Kaunas, Lithuania.
3. Report of PSRC Working Group D15. High Impedance Fault Detection Technology. March 1996.
4. Girgis A, Chang W, Makram E. Analysis of high-impedance fault generated signals using a Kalman filtering approach. *IEEE Transactions on Power Delivery* 1990; **5**(5):1714–1724.
5. Mamishev A, Russell B, Benner G. Analysis of high impedance faults using fractal techniques. *IEEE Transactions on Power Delivery* 1996; **11**(1):435–440.
6. Sedighi A, Haghifam M, Malik O, Ghassemian M. High impedance fault detection based on wavelet transform and statistical pattern recognition. *IEEE Transactions on Power Delivery* 2005; **20**(4):1414–2421.
7. Wai D, Yibin X. A novel technique for high impedance fault identification. *IEEE Transactions on Power Delivery* 1998; **13**(3):738–744.
8. Russell B, Benner C. Arcing fault detection for distribution feeders: security assessment in long term field trials. *IEEE Transactions on Power Delivery* 1995; **10**(2):676–683.
9. Jeeringes D, Linders J. Unique aspects of distribution system harmonics due to high impedance ground faults. *IEEE Transactions on Power Delivery* 1990; **5**(2):1086–1094.
10. Benner G, Russell B. Practical high-impedance fault detection on distribution feeders. *IEEE Transactions on Industry Applications* 1997; **33**(3):635–640.
11. Lehtonen M, Hakola T. Neutral Earthing and Power System Protection. Earthing Solutions and Protective Relaying in Medium Voltage Distribution Networks. *ABB Transmit Oy*, FIN-65101 Vassa, Finland, 1996.
12. Nordman M, Korhonen T. Design of a concept and a wireless ASIC sensor for locating earth faults in unearthed electrical distribution networks. *IEEE Transactions on Power Delivery* 2006; **21**(3):1074–1082.
13. Fernandes R. Electrical Power Line and Substation Monitoring Apparatus and Systems. European Patent Applicat 0314849, May 10, 1989.
14. Vähämäki O, Rautiainen K, Kauhaniemi K. Measurement of Quantities of Electric Line. Patent Applicat WO0171367, September 27, 2001.

15. Vieira M, Coelho C, da Silva D, da Mata J. Survey on Wireless Sensor Network Devices. *Emerging Technologies and Factory Automation ETFA'03*, 16–19 September 2003; 537–544
16. Prikler L, Hoildalen H. ATPDraw users' manual. SINTEF TR A4790, November 1998.
17. Kizilcay M, Pniok T. Digital simulation of fault arcs in power systems. *Europe Transaction on Electrical Power System* 1991; 4(3):55–59.
18. Darwish H, Elkalashy N. Universal arc representation using EMTP. *IEEE Transactions on Power Delivery* 2005; 2(2):774–779.
19. Solanki M, Song Y, Potts S, Perks A. Transient protection of transmission line using wavelet transform. *Seventh International Conference on Developments in Power System Protection, (IEE) 9–12 April 2001*; 299–302.
20. Darwish H, Farouk M, Taalab A, Mansour N. Investigation of Real-Time Implementation of DSP-Based DWT for Power System Protection. *IEEE/PES Transmission and Distribution Conference and Exposition* May 21–26, 2006, Dallas, Texas, USA.
21. Wavelet Toolbox for MATLAB, Math Works 2005.

AUTHORS' BIOGRAPHIES



Nagy I. Elkalashy (S'06) was born in Quesna, Egypt on August 4, 1974. He received the B.Sc. (with first class honours) and M.Sc. degrees from the Electrical Engineering Department, Faculty of Engineering, Shebin El-Kom, Menoufiya University in 1997 and 2002, respectively. Currently, he is working towards the Ph.D. at Power Systems and High Voltage Engineering, Helsinki University of Technology (TKK), Finland under joint supervision with Menoufiya University. His research interests are high-impedance fault detection, power system transient studies including AI, EMTP simulation, and switchgear.



Matti Lehtonen (1959) was with VTT Energy, Espoo, Finland from 1987 to 2003, and since 1999 has been a Professor at the Helsinki University of Technology, where he is now head of Power Systems and High Voltage Engineering. Matti Lehtonen received both his Master's and Licentiate degrees in Electrical Engineering from Helsinki University of Technology, in 1984 and 1989, respectively, and the Doctor of Technology degree from Tampere University of Technology in 1992. The main activities of Dr Lehtonen include power system planning and asset management, power system protection including earth fault problems, harmonic related issues and applications of information technology in distribution systems.



Hatem A. Darwish (M'06-SM'06) was born in Quesna, Egypt on September 13, 1966. He received his B.Sc. (honours), M.Sc. degrees, and Ph.D. in Electrical Engineering, Menoufiya University, Egypt in 1988, 1992 and 1996, respectively. From 1994 to 1996, he was working towards the Ph.D. at Memorial University of Newfoundland (MUN), St. John's, Canada based on Joint Supervision with Menoufiya University. He has been involved in several pilot projects for the Egyptian industry for the design and implementation of numerical relays, SCADA, fault location in MV feeders, distribution management systems, protection training packages, and relay coordination. Dr Darwish is currently a visiting Professor at the University of Calgary. His interests are in digital protection, signal processing, system automation, and EMTP ac/dc simulation, and switchgear.



Abdel-Maksoud I. Taalab (M'99–SM'03) received his B.Sc. degree in 1969, in Electrical–Engineering from Menoufiya University, Egypt, M.Sc. degrees and Ph.D. from Manchester University, U.K., in 1978 and 1982, respectively. In the same year of his graduation, he was appointed as an Assistant Professor at the Menoufiya University. He joined GEC Company in 1982. He is now a full Professor at the department of Electrical Engineering, Faculty of Engineering and vice dean of the Desert Environment Institute, Menoufiya University. His interests are in hvdc transmission systems, power system protection, and power electronics applications.



Mohamed A. Izzularab was born in Tanta, Egypt on 1950. He received his B.Sc. degree in Electrical Engineering from Menoufiya University, Egypt in 1973. He was awarded the M.Sc. degree from Elmansoura University in 1978 and Dr -Ing degree from I.N.P.T. Toulouse, France in 1983. Also he was awarded the D.Sc. in Electrical Engineering from Paul Sabatier University Toulouse, France in 1987. He obtained the Cigre Award for the best-applied research for the year 1998. Dr Izzularab is the vice dean of the Faculty of Engineering, Menoufiya University.